



Universidade de São Paulo

Biblioteca Digital da Produção Intelectual - BDPI

Departamento de Física e Ciência Interdisciplinar - IFSC/FCI

Artigos e Materiais de Revistas Científicas - IFSC/FCI

2014

Interband polarized absorption in InP polytypic superlattices

Journal of Applied Physics, College Park : American Institute of Physics - AIP, v. 116, n. 19, p.

193501-1-193501-8, 2014

<http://www.producao.usp.br/handle/BDPI/50703>

Downloaded from: Biblioteca Digital da Produção Intelectual - BDPI, Universidade de São Paulo

Interband polarized absorption in InP polytypic superlattices

P. E. Faria Junior, T. Campos, and G. M. Sipahi

Citation: *Journal of Applied Physics* **116**, 193501 (2014); doi: 10.1063/1.4901209

View online: <http://dx.doi.org/10.1063/1.4901209>

View Table of Contents: <http://scitation.aip.org/content/aip/journal/jap/116/19?ver=pdfcov>

Published by the [AIP Publishing](#)

Articles you may be interested in

Proposal of high efficiency solar cells with closely stacked InAs/In_{0.48}Ga_{0.52}P quantum dot superlattices: Analysis of polarized absorption characteristics via intermediate-band
Appl. Phys. Lett. **105**, 011120 (2014); 10.1063/1.4889805

Polarization dependent study of gain anisotropy in semipolar InGaN lasers
Appl. Phys. Lett. **99**, 171105 (2011); 10.1063/1.3655183

White light emission from p-doped quaternary (AlInGa)N-based superlattices: Theoretical calculations for the cubic phase
J. Appl. Phys. **101**, 113706 (2007); 10.1063/1.2737968

Intervalence band absorption in InP and related materials for optoelectronic device modeling
J. Appl. Phys. **87**, 1054 (2000); 10.1063/1.371979

Experimental and theoretical density-dependent absorption spectra in (GaInSb/InAs)/AlGaSb superlattice multiple quantum wells
Appl. Phys. Lett. **72**, 229 (1998); 10.1063/1.120694

An advertisement for Asylum Research Cypher AFMs. The background is dark blue with a film strip graphic on the left. The text is in white and orange. The Oxford Instruments logo is in the bottom right corner.

Not all AFMs are created equal
Asylum Research Cypher™ AFMs
There's no other AFM like Cypher

www.AsylumResearch.com/NoOtherAFMLikeIt

OXFORD
INSTRUMENTS
The Business of Science®

Interband polarized absorption in InP polytypic superlattices

P. E. Faria Junior,^{1,2} T. Campos,¹ and G. M. Sipahi^{1,2}

¹Instituto de Física de São Carlos, Universidade de São Paulo, 13566-590 São Carlos, São Paulo, Brazil

²Department of Physics, State University of New York at Buffalo, Buffalo, New York 14260, USA

(Received 25 September 2014; accepted 25 October 2014; published online 17 November 2014)

Recent advances in growth techniques have allowed the fabrication of semiconductor nanostructures with mixed wurtzite/zinc-blende crystal phases. Although the optical characterization of these polytypic structures is well reported in the literature, a deeper theoretical understanding of how crystal phase mixing and quantum confinement change the output linear light polarization is still needed. In this paper, we theoretically investigate the mixing effects of wurtzite and zinc-blende phases on the interband absorption and in the degree of light polarization of an InP polytypic superlattice. We use a single 8×8 k-p Hamiltonian that describes both crystal phases. Quantum confinement is investigated by changing the size of the polytypic unit cell. We also include the optical confinement effect due to the dielectric mismatch between the superlattice and the vacuum and we show it to be necessary to match experimental results. Our calculations for large wurtzite concentrations and small quantum confinement explain the optical trends of recent photoluminescence excitation measurements. Furthermore, we find a high sensitivity to zinc-blende concentrations in the degree of linear polarization. This sensitivity can be reduced by increasing quantum confinement. In conclusion, our theoretical analysis provides an explanation for optical trends in InP polytypic superlattices, and shows that the interplay of crystal phase mixing and quantum confinement is an area worth exploring for light polarization engineering. © 2014 AIP Publishing LLC. [<http://dx.doi.org/10.1063/1.4901209>]

I. INTRODUCTION

The past few years has seen tremendous advances in growth techniques of low dimensional semiconductor nanostructures, especially concerning III-V nanowires (NWs). At the moment, it is possible to precisely tune the growth conditions to achieve single crystal phase nanostructures^{1–3} or polytypic heterostructures with sharp interfaces.^{4,5} Moreover, it has been reported successful integration of III-V NWs with silicon,^{6–9} increasing the possibilities for developing new optoelectronic devices.^{10,11}

Because of its lower surface recombination and higher electron mobility,^{12,13} InP is a good candidate, among the III-V compounds, to be embedded in these novel devices. Polytypic InP homojunctions showing a type-II band alignment¹⁴ can be explored to engineer light polarization¹⁵ and to enhance the lifetime of carriers.^{16,17} In fact, the use of InP NWs has been proposed in FETs,^{18–20} silicon integrated nanolasers,²¹ and stacked p-n junctions in solar cells.^{22,23}

Although the process underlying the formation of these polytypic homojunctions is elucidated^{24–27} and an extensive literature on the optical characterization of these structures is available,^{9,28–32} we lack theoretical understanding of how the crystal phase mixture changes the light polarization on these nanostructures.

The aim of this study is to provide a comprehensive analysis on how wurtzite (WZ)/zinc-blende (ZB) mixing, quantum confinement (QC), and also optical confinement (OC) modify the interband absorption and the degree of linear polarization (DLP) in an InP polytypic superlattice. From now on, we will use the term superlattice for the polytypic case. In our calculations, the QC along growth direction takes into account the changes of WZ and ZB phases. Also, assuming large cross-sections, we neglect lateral QC.

A scheme of the superlattice and possible light polarization is presented in Fig. 1(a). Although we show a NW with multiple WZ and ZB segments, the periodicity of these segments allows us to consider only the unit cell, bounded by dashed lines, to understand the physics of the superlattice. The incoming light polarization can be either parallel (Z) or perpendicular (X) to the growth direction.

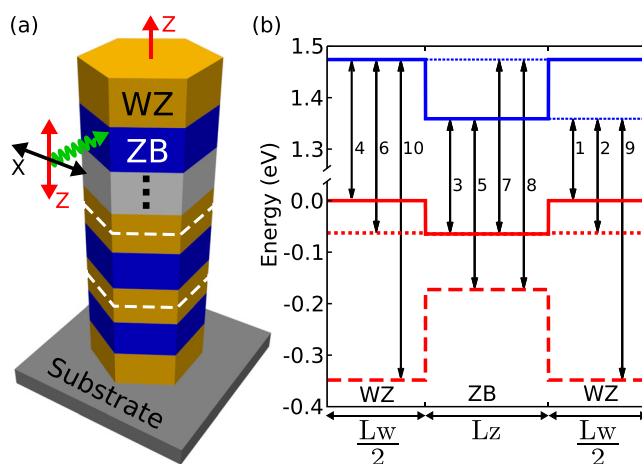


FIG. 1. (a) InP polytypic superlattice grown along WZ[0001]/ZB[111] direction. The (red) arrow on top indicates the growth direction. Polarization of incident light can be in X- or Z-direction, i.e., perpendicular or parallel to the growth direction. The polytypic superlattice unit cell, of size $L = L_w + L_z$ is bounded by dashed (white) lines. (b) Band-edge energy diagram at $\vec{k} = 0$ of type-II InP supercell with possible transitions. The numbers on the side of the vertical arrows indicate the magnitude of energy transitions, i.e., 1 means the lowest and 10 the highest. For the valence band, solid line is heavy hole band for both WZ/ZB, dotted line is light hole band for both WZ/ZB, and dashed line is crystal-field split-off hole band for WZ and split-off hole band for ZB. The small dotted lines in the conduction band are plotted just to guide the eyes.

To calculate the band structure, we extend our polytypic k-p method³³ and include the conduction and valence band interaction explicitly. This interaction increases the reliability of the method, and allows us to calculate the band structure further away from the center of the Brillouin zone. Furthermore, we provide the parameter sets for WZ and ZB InP in this new 8×8 k-p configuration.

We find that the trends of recent photoluminescence (PL) and excitation photoluminescence (PLE) measurements performed by Gadret *et al.*³¹ can be explained by our model. Although their samples are disordered, i.e., the regions of WZ/ZB are not periodically ordered, we can predict the observed trends considering a supercell of 100 nm composed of 95% WZ. In addition, we show that the DLP can be tuned using WZ/ZB mixing and QC. The limiting cases of our superlattice, i.e., pure ZB and pure WZ NWs are also calculated and their DLP around gap energy is in very good agreement with the results from Mishra *et al.*²⁹ This matching emphasizes the use of OC in our calculations.

The structure of the present paper is the following: In Sec. II, we describe the 8×8 polytypic k-p method and present our approach for the interband transitions. Section III contains our results for interband absorption and DLP in the bulk and superlattice regimes. Finally, in Sec. IV, we summarize our main findings and present our conclusions.

II. THEORETICAL BACKGROUND

A. Hamiltonian

We expand the Hamiltonian of Ref. 33 to explicitly include the interband interaction. Since there is no coupling between the ZB irreducible representations for conduction ($\Gamma_1 \sim x^2 + y^2 + z^2$) and valence ($\Gamma_{15} \sim x, y, z$) bands, we can apply the same rotation³⁴ for the [001] k-p matrix with interband interaction. The total rotation matrix would be the direct sum of valence and conduction band rotation matrices, therefore an 8×8 matrix with 6×6 and 2×2 blocks. An alternative procedure would be to start with the Hamiltonian in the [111] coordinate system without interband interaction and derive the interband matrix elements in the [111] coordinate system relating them to the [001].

Our bulk Hamiltonian basis set, defined at Γ -point, in the ZB[111]/WZ[0001] coordinate system is

$$\begin{aligned} |c_1\rangle &= -\frac{1}{\sqrt{2}}|(X+iY)\uparrow\rangle \\ |c_2\rangle &= \frac{1}{\sqrt{2}}|(X-iY)\uparrow\rangle \\ |c_3\rangle &= |Z\uparrow\rangle \\ |c_4\rangle &= \frac{1}{\sqrt{2}}|(X-iY)\downarrow\rangle \\ |c_5\rangle &= -\frac{1}{\sqrt{2}}|(X+iY)\downarrow\rangle \\ |c_6\rangle &= |Z\downarrow\rangle \\ |c_7\rangle &= i|S\uparrow\rangle \\ |c_8\rangle &= i|S\downarrow\rangle \end{aligned} \quad (1)$$

with 1-6 representing the valence band states and 7-8 the conduction band states. In this basis set, the Hamiltonian including interband interactions is given by

$$\mathbb{H}_8 = \begin{bmatrix} \mathbb{H}_V & \mathbb{H}_{VC} \\ \mathbb{H}_{VC}^\dagger & \mathbb{H}_C \end{bmatrix}, \quad (2)$$

where \mathbb{H}_V represent the valence band, \mathbb{H}_C is the conduction band, and \mathbb{H}_{VC} is the interaction term between them. The sub-matrices have the following forms:

$$\mathbb{H}_V = \begin{bmatrix} F & -K^* & -H^* & 0 & 0 & 0 \\ -K & G & H & 0 & 0 & \sqrt{2}\Delta_3 \\ -H & H^* & \lambda & 0 & \sqrt{2}\Delta_3 & 0 \\ 0 & 0 & 0 & F & -K & H \\ 0 & 0 & \sqrt{2}\Delta_3 & -K^* & G & -H^* \\ 0 & \sqrt{2}\Delta_3 & 0 & H^* & -H & \lambda \end{bmatrix}, \quad (3)$$

$$\mathbb{H}_{VC} = \begin{bmatrix} -\frac{1}{\sqrt{2}}P_2k_- & 0 \\ \frac{1}{\sqrt{2}}P_2k_+ & 0 \\ P_1k_z & 0 \\ 0 & \frac{1}{\sqrt{2}}P_2k_+ \\ 0 & -\frac{1}{\sqrt{2}}P_2k_- \\ 0 & P_1k_z \end{bmatrix}, \quad (4)$$

$$\mathbb{H}_C = \begin{bmatrix} E_C & 0 \\ 0 & E_C \end{bmatrix} \quad (5)$$

and their terms

$$\begin{aligned} F &= \Delta_1 + \Delta_2 + \lambda + \theta, \\ G &= \Delta_1 - \Delta_2 + \lambda + \theta, \\ \lambda &= \tilde{A}_1k_z^2 + \tilde{A}_2(k_x^2 + k_y^2), \\ \theta &= \tilde{A}_3k_z^2 + \tilde{A}_4(k_x^2 + k_y^2), \\ K &= \tilde{A}_5k_+^2 + 2\sqrt{2}\tilde{A}_zk_-k_z, \\ H &= \tilde{A}_6k_+k_z + \tilde{A}_zk_-^2, \\ E_C &= E_g + E_0 + \tilde{e}_1k_z^2 + \tilde{e}_2(k_x^2 + k_y^2), \end{aligned} \quad (6)$$

where $\tilde{A}_1 \dots \tilde{A}_6, \tilde{A}_z$ and \tilde{e}_1, \tilde{e}_2 , given in units of $\hbar^2/2m_0$, are the effective mass parameters of valence and conduction bands, respectively. Here Δ_1 is the crystal field splitting energy in WZ, Δ_2, Δ_3 are the spin-orbit coupling splitting energies, $k_\pm = k_x \pm ik_y$ and P_1, P_2 are the Kane parameters of the interband interactions, given by

$$\begin{aligned}
P_1 &= -i \frac{\hbar}{m_0} \langle X | p_x | S \rangle = -i \frac{\hbar}{m_0} \langle Y | p_y | S \rangle, \\
P_2 &= -i \frac{\hbar}{m_0} \langle Z | p_z | S \rangle.
\end{aligned} \quad (7)$$

We would like to emphasize that the Hamiltonian (2) and its terms (6) describe both WZ and ZB crystal structures, however, the usual ZB parameters must be mapped to the ones in Eq. (6). Moreover, the inclusion of the interband interaction explicitly in the Hamiltonian also requires some corrections to be made in the second order effective mass parameters. These corrections appear because conduction and valence band states are now treated as belonging to the same class, following Löwdin's notation.³⁵ We describe the mapping and corrections of parameters with detail in the Appendix.

In order to treat the confined direction along z , we apply the envelope function approximation^{36,37} to the Hamiltonian (2). This treatment can be summarized with the following changes:

$$\begin{aligned}
g &\rightarrow g(z) \\
k_z &\rightarrow -i \frac{\partial}{\partial z} \\
Bk_z^2 &\rightarrow -\frac{\partial}{\partial z} B(z) \frac{\partial}{\partial z} \\
Pk_z &\rightarrow -\frac{i}{2} \left[\frac{\partial}{\partial z} P(z) + P(z) \frac{\partial}{\partial z} \right]
\end{aligned} \quad (8)$$

with g representing the parameters in the Hamiltonian (different in WZ and ZB), B representing an effective mass parameter and P is the interband parameter. The last two equations are the symmetrization requirements to hold the Hermitian property of the momentum operator.³⁷ Any parameter in the Hamiltonian acquires a dependence along z , making it different for WZ and ZB. Also, the confinement profile due to the polytypic interface is added to the Hamiltonian. In Fig. 1(b), we present the InP band-edge profile along z for $k = 0$, which takes into account the interface profile and the intrinsic splittings of each crystal structure.

Under the envelope function approximation, a general state n, \vec{k} of the superlattice can be written as

$$\psi_{n,\vec{k}}(\vec{r}) = e^{i\vec{k}\cdot\vec{r}} \sum_{m=1}^8 f_{n,\vec{k},m}(z) u_m(\vec{r}). \quad (9)$$

We then apply the plane wave expansion for the parameters and the envelope functions to solve the Hamiltonian numerically. Since this expansion automatically considers periodic boundary conditions, we can associate the value k_z for the superlattice, $-\frac{\pi}{L} \leq k_z \leq \frac{\pi}{L}$, while the Fourier coefficients have $K_j = j \frac{2\pi}{L}$ (with $j = 0, \pm 1, \pm 2, \dots$). For confined states, the dispersion of the band structure along k_z is a flat band. However, higher energy states are no longer confined and does not have this flat dispersion. Since we are interested in transitions that also take into account these higher energy states, we will include the k_z in our calculation.

B. Interband absorption

The absorption coefficient³⁸ of photons with energy $\hbar\omega$ can be written as

$$\alpha_\epsilon(\hbar\omega) = \frac{C}{\hbar\omega} \sum_{a,b,\vec{k}} I_{a,b,\vec{k}}^\epsilon (f_{a,\vec{k}} - f_{b,\vec{k}}) \mathcal{L}_{a,b,\vec{k}}^\Gamma(\hbar\omega), \quad (10)$$

where a (b) runs over conduction (valence) sub-bands, \vec{k} runs over reciprocal space points, $\hat{\epsilon}$ is the light polarization, $I_{a,b,\vec{k}}^\epsilon$ is the interband dipole transition amplitude, $\mathcal{L}_{a,b,\vec{k}}^\Gamma(\hbar\omega)$ gives the transition broadening, and $f_{a(b),\vec{k}}$ is the Fermi-Dirac distribution of conduction (valence) band. We will consider $T = 0$ K and no doping, i.e., the valence band is full and the conduction band is empty,³⁹ leading to $f_{a,\vec{k}} - f_{b,\vec{k}} = 1$. The constant C is given by

$$C = \frac{\pi \hbar e^2}{c n_r \epsilon_0 m_0^2 \Omega}, \quad (11)$$

where e is the electron charge, c is the velocity of light, n_r is the refractive index of the material, ϵ_0 is the vacuum dielectric constant, m_0 is the free electron mass, and Ω is the volume of the real space.

We considered a Lorentzian broadening for the transitions

$$\mathcal{L}_{a,b,\vec{k}}^\Gamma(\hbar\omega) = \frac{1}{2\pi} \frac{\Gamma}{[E_a(\vec{k}) - E_b(\vec{k}) - \hbar\omega]^2 + (\frac{\Gamma}{2})^2} \quad (12)$$

with Γ as the full width at half-maximum. In our calculations, we set $\Gamma = 2$ meV.

For \hat{x} and \hat{z} light polarizations, the interband dipole transition amplitudes, between conduction (a) and valence (b) states, are given by

$$\begin{aligned}
I_{a,b,\vec{k}}^{\hat{x}} &\propto \frac{1}{2} |\langle F_{a,\vec{k},7} | F_{b,\vec{k},1} \rangle + \langle F_{a,\vec{k},1} | F_{b,\vec{k},7} \rangle \\
&\quad - \langle F_{a,\vec{k},7} | F_{b,\vec{k},2} \rangle - \langle F_{a,\vec{k},2} | F_{b,\vec{k},7} \rangle \\
&\quad - \langle F_{a,\vec{k},8} | F_{b,\vec{k},4} \rangle - \langle F_{a,\vec{k},4} | F_{b,\vec{k},8} \rangle \\
&\quad + \langle F_{a,\vec{k},8} | F_{b,\vec{k},5} \rangle + \langle F_{a,\vec{k},5} | F_{b,\vec{k},8} \rangle|^2,
\end{aligned} \quad (13)$$

$$\begin{aligned}
I_{a,b,\vec{k}}^{\hat{z}} &\propto |\langle F_{a,\vec{k},7} | F_{b,\vec{k},3} \rangle + \langle F_{a,\vec{k},3} | F_{b,\vec{k},7} \rangle \\
&\quad + \langle F_{a,\vec{k},8} | F_{b,\vec{k},6} \rangle + \langle F_{a,\vec{k},6} | F_{b,\vec{k},8} \rangle|^2
\end{aligned} \quad (14)$$

with

$$\langle F_{a,\vec{k},m} | F_{b,\vec{k},n} \rangle = \frac{1}{L} \int_L dz f_{a,\vec{k},m}^*(z) f_{b,\vec{k},n}(z), \quad (15)$$

where L is the size of the supercell and the factor $1/L$ appears because our envelope functions are normalized in reciprocal space.

We assumed the interband coupling parameters to be constant throughout the polytypic system, i.e., the same values were used for both polytypes since their numerical values do not differ much (see Table I).

The relative contributions of the different light polarizations can be probed by analyzing the DLP:

TABLE I. k-p parameters of the polytypic 8×8 model for InP.

Parameter	ZB InP	WZ InP
Lattice constant (\AA)		
a	4.1505	4.1505
c	10.1666	6.7777
Energy parameters (eV)		
E_g	1.4236	1.474
Δ_1	0	0.303
$\Delta_2 = \Delta_3$	0.036	0.036
Conduction band effective mass parameters (units of $\frac{\hbar^2}{2m_0}$)		
\tilde{e}_1	-1.6202	-1.2486
\tilde{e}_2	-1.6202	-1.6231
Valence band effective mass parameters (units of $\frac{\hbar^2}{2m_0}$)		
\tilde{A}_1	1.0605	0.0568
\tilde{A}_2	-0.8799	-0.8299
\tilde{A}_3	-1.9404	-0.8423
\tilde{A}_4	0.9702	1.2001
\tilde{A}_5	1.4702	11.4934
\tilde{A}_6	2.7863	9.8272
\tilde{A}_z	-0.5000	0
Interband coupling parameters (eV \AA)		
$P_1 = P_2$	8.7249	8.3902

$$\text{DLP}(\hbar\omega) = \frac{\alpha_z(\hbar\omega) - \alpha_x(\hbar\omega)}{\alpha_z(\hbar\omega) + \alpha_x(\hbar\omega)} \quad (16)$$

which ranges from -1 , if the absorbed light is polarized perpendicular to the wire axis, to 1 , if polarization is parallel to the growth direction.

We have also investigated the effect of OC due to the dielectric mismatch between the vacuum and the superlattice. This effect is included as follows:⁴⁰

$$\alpha_{\hat{x}}(\hbar\omega) \rightarrow \frac{2}{1 + \epsilon} \alpha_{\hat{x}}(\hbar\omega) \quad (17)$$

with ϵ being the dielectric constant of the superlattice, which was considered to be the same for ZB and WZ InP ($\epsilon = 12.4$ (Refs. 41 and 42)).

III. RESULTS AND DISCUSSION

A. Bulk

Before we turn to the superlattice case, it is useful to understand the light polarization properties for bulk ZB and WZ. Indeed, these would be the limiting cases of our superlattice calculations. We can view these bulk limiting cases as NWs of large diameter and length, with pure crystal phases. Here, we also assumed the light polarizations described in Fig. 1(a). Moreover, the 8×8 parameter sets were derived from the 6×6 model of our previous paper,³³ which was based on the effective masses of Ref. 43. The lattice constants a and c of ZB are given in the [111] unit cell (ZB has three bilayers of atoms instead of two in WZ). Table I have all the parameters used in the simulations.

In Fig. 2(a), we show the band structure of bulk ZB[111] and WZ[0001] for k_x and k_z directions. At $\vec{k} = 0$,

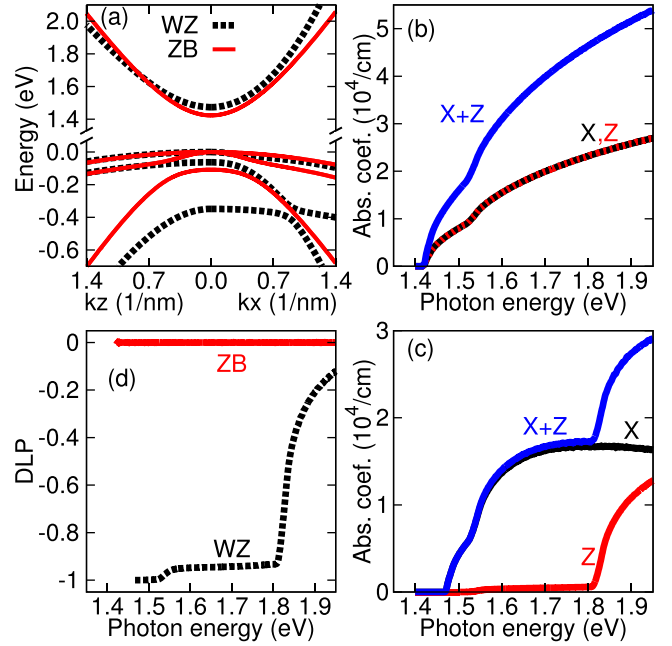


FIG. 2. In clockwise order: (a) InP bulk band structure for WZ (dashed lines) and ZB (solid lines). InP Bulk ZB (b) and WZ (c) absorption coefficients as functions of the photon energies. (d) ZB (solid line) and WZ (dashed line) DLP. The crystal structure plays an important role in the absorption: ZB absorbs light isotropically, while WZ have a clear anisotropy that changes when photon energy reaches the band edge energies.

the valence band of WZ has three energy bands two-fold degenerate, while ZB has one four-fold degenerate band and one two-fold degenerate. From top to bottom, WZ valence bands are labeled HH (heavy hole), LH (light hole), and CH (crystal-field split-off hole), following Chuang and Chang's notation,⁴⁴ and ZB valence bands are labeled usually as HH/LH and SO (split-off hole). Each band-edge in the band structure will have a signature in the absorption spectra; therefore, we can expect three regions for WZ and only two for ZB. Moreover, the symmetry of the eigenstates will rule the light polarization, as shown by Eqs. (13) and (14).

Figures 2(b) and 2(c) show the bulk absorption coefficients for ZB and WZ, respectively, as calculated by Eq. (10). Although we considered ZB in the [111] unit cell, X- and Z-polarizations have the same absorption as we would expect from the cubic symmetry. One can easily show that the coordinate system rotation we have applied holds this cubic character in the absorption coefficient. Note the shoulder in the curve when the photon energy reaches the SO band energy. For WZ, however, a clear anisotropy between X- and Z-polarizations is found. Before we reach the CH band energy, light is predominantly X-polarized, however, after CH band the Z-polarized absorption increases while X-polarized slightly decreases.

To highlight the polarization differences for ZB and WZ, we show in Fig. 2(d) the DLP, given by Eq. (16). Since X- and Z-polarizations are the same in ZB, we have a straight line at $\text{DLP} = 0$, meaning isotropic absorption. For WZ, the DLP starts at -1 , slightly increases when LH band is reached and after CH band, it rapidly goes to 0 due to the Z-polarization contribution. In the superlattice calculations, we expect that the WZ/ZB mixing and QC effects will

change the DLP to some intermediate value between pure ZB and WZ.

B. Absorption and PLE measurements

Let us start the superlattice investigation by considering small QC, i.e., relatively large WZ and ZB regions (5–90 nm each with total supercell of 100 nm), values typically found in superlattice samples. Although there is small QC, small regions of WZ and ZB act as perturbations to the bulk states leading to different electronic and optical properties.

In Fig. 3(a), we show the total absorption, $\alpha_x + \alpha_z$, without OC effects. The first (top) solid curve is the case of 90% of ZB and 10% of WZ and we can notice the two characteristic shoulders of the bulk case, the first around transition energy 3 and the second around transition 5. Increasing the mixing of ZB and WZ, new shoulders appear and when we reach the last (bottom) solid curve, 90% of WZ and 10% of ZB, we notice the three characteristic shoulders of WZ bulk case, around transitions 4, 6, and 10, respectively. This WZ characteristic is also noted in the dashed line, which is the 95%WZ/5%ZB. We can also notice from Fig. 3(a) that there is a non-zero absorption coefficient between ZB and WZ energy gaps (transitions 2 and 4) even for large WZ concentrations. This phenomenon is due to the characteristic type-II band alignment of ZB/WZ homojunctions.

When we add OC effects, which are presented in Fig. 3(b), we notice a significant suppression of X-polarization that becomes more evident as WZ/ZB ratio increases. Since

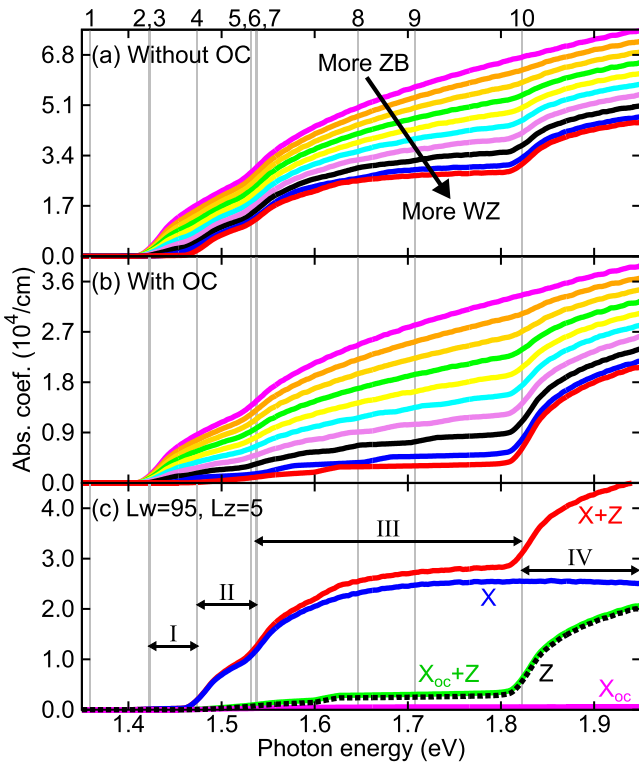


FIG. 3. Absorption coefficient for 100 nm supercell with different WZ/ZB ratio (a) without OC and (b) with OC. From top to bottom, solid lines range from 10%WZ/90%ZB to 90%WZ/10%ZB with steps of 10%. The dashed line is the 95%WZ/5%ZB regime. (c) Absorption coefficient for 95%WZ/5%ZB, including the contributions for X- and Z-polarizations. The numbers at the top of the figure indicate the transition energies of Fig. 1(b).

in WZ, the absorption spectrum in regions I and II is mainly comprises sub-bands with a mixture of states $|c_1\rangle, |c_4\rangle$ due to HH symmetry, the OC almost forbids the X component from penetrating the NW, therefore the suppression.

The experimental paper of Gadret *et al.*³¹ investigates optical properties of InP polytypic superlattices. They report PL and PLE measurements of InP polytypic samples with statistically negligible percentage of ZB. In this regime, they notice three absorption edges in the PLE (~ 1.488 eV, ~ 1.532 eV, and ~ 1.675 eV) for energies above the PL peak (~ 1.432 eV) and also a long tail at the low energy side of the PL peak. Their system is comparable to our simulation for 100 nm supercell with 95% of WZ and 5% of ZB or even higher WZ percentage over ZB. Indeed, the measured trends are well described by our Fig. 3(c). We can identify four regions that we can relate to the experimental spectra: I (between transitions 2/3 and 4, i.e., between ZB and WZ gap energies), II (between transitions 4 and 5/6/7), III (between transitions 5/6/7 and 10), and IV (after transition 10). From the observed data, we can assign the three absorption edges to the beginning of energy regions II, III, and IV, respectively. Region I actually comprises the region where the PL peak is observed. Furthermore, the long tail at low energy side of PL can be explained by the type-II confinement of WZ/ZB interface, which has negligible absorption coefficient. Since we are not considering excitons, we do not observe the peaks in the absorption at the band-edge transitions (visible in the experimental data). However, the band-edge character is well described by our model, represented by the shoulders in our graphs. The blue-shift of our band-edge transition energies compared to the experimental data is also related to the lack of excitonic effects in our model.

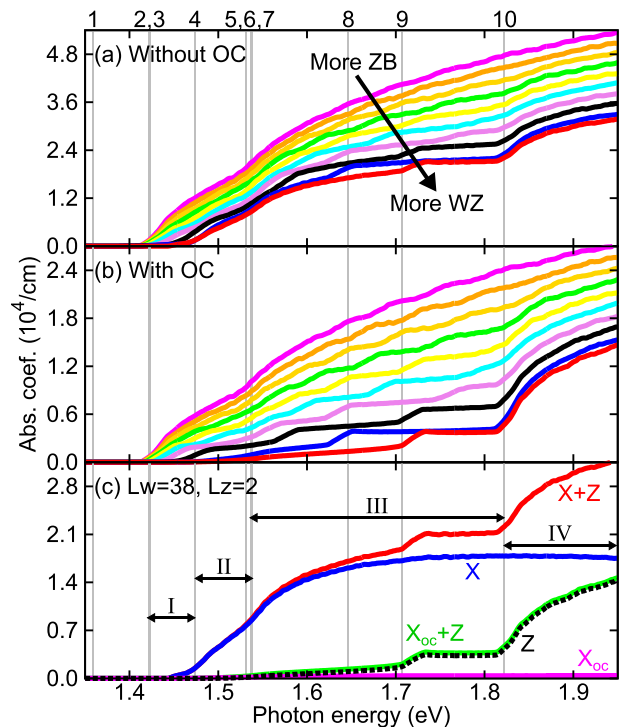


FIG. 4. Same as system Fig. 3 for 40 nm supercell. In this case, because of the smaller supercell, QC effects are more pronounced.

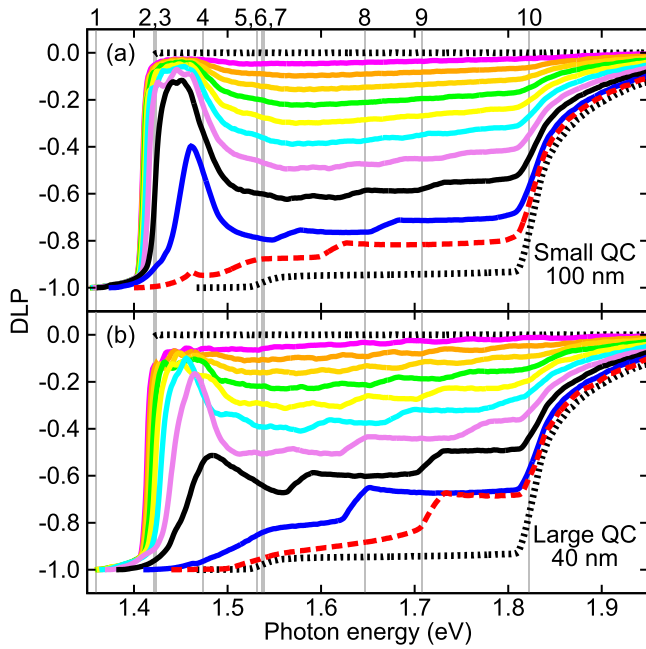


FIG. 5. Degree of linear polarization without optical confinement for small QC (a) and large QC (b). The straight dotted line at 0 indicates the bulk ZB limit, whereas the lowest dotted line is the bulk WZ limit. The solid and dashed lines have the same meaning as in Figs. 3 and 4.

For comparison, we plotted in Fig. 4 the same results but for a 40 nm supercell. In Figs. 4(a) and 4(b), we observe the same trends as before but with more quantization effects, signalled by the extra shoulders or step-like behavior in absorption spectra. As we increase the QC, the number of sub-bands in the same energy range decreases, leading to clear shoulders in the spectra as the photon energy reaches these few sub-bands. In Fig. 4(c), we show the different contribution of X- and Z-polarizations. Comparing to Fig. 3(c), it can be seen that the QC effect is more visible in Z-polarization since this is the confined direction. For the X-polarization, a small red-shift is observed due to greater overlap between states.

C. Quantum confinement and crystal phase mixing effects in the DLP

For a better understanding of the optical properties of the InP homojunctions, it is valuable to study the DLP. Specifically, we are interested in how polarization properties are modified by different crystal phase mixing and QC.

In Fig. 5, we show the behavior of the DLP only under QC effects, no OC included, for the case in which the supercell has 100 nm, Fig. 5(a), and 40 nm, Fig. 5(b). In general, the DLP is very sensitive to ZB insertions: In region I, it is close to 0, exception made to systems where WZ regions are largely dominant over ZB ones, about 80%WZ or more for the small QC regime and 70%WZ or more in large QC. For all different WZ/ZB mixing, the limits are bulk WZ and bulk ZB DLP, presented in Fig. 2(d) and showed here with dotted lines.

To further analyze the effect of the OC, we present in Fig. 6 the DLP calculations for the same systems previously discussed, including QC and OC effects. Here, we also include OC effects in bulk calculations. In the paper of

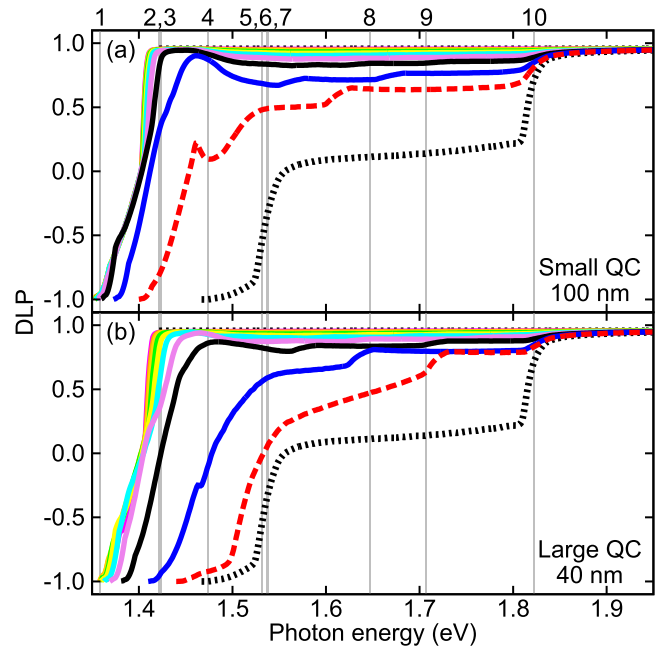


FIG. 6. Same as Fig. 5 but including optical confinement. The straight dotted line at 1 indicates the bulk ZB limit, whereas the lowest dotted line is the bulk WZ limit.

Mishra *et al.*,²⁹ their PL measurements for pure WZ and ZB NWs with large diameters indicate that for ZB light is strongly polarized along the NW axis, whereas for WZ light is strongly polarized in the perpendicular direction. Our calculations for the bulk case with OC are in very good agreement with these experimental results. In fact, this indicates that OC is a necessary feature to be included in the description. Also, these are the limiting cases for all WZ/ZB mixed systems.

Comparing the results with OC for small QC, Fig. 6(a), and large QC, Fig. 6(b), we also notice that the DLP is very susceptible to ZB concentration, i.e., just a small amount of ZB can switch the DLP from -1 to approximately 1 . Moreover, for large QC, WZ features hold more effectively around the gap energy. This happens because WZ holes (parallel to growth direction) have larger effective masses ($m_{HH}^{ZB} = 0.532$ and $m_{HH}^{WZ} = 1.273$) and, therefore, are the dominant symmetry to light polarization. Hence, increasing QC can reduce the ZB susceptibility to the DLP.

As a final remark, if we compare our DLP for small QC to the PL spectra measurement of Gadret *et al.*,³¹ we also notice a non-zero value for parallel polarization. Since their NWs have a statistically negligible percentage of ZB and still present parallel polarization, we believe that this corroborates our results of ZB susceptibility to the DLP.

IV. CONCLUSIONS

We have expanded our previous polytypic k-p model³³ to include interband coupling explicitly. The validation of our 8×8 model was considered for the bulk case, and we found how selection rules for WZ and ZB allow different light polarization features.

For the InP polytypic superlattice, we found good agreement between our results and the experimental

measurements of PLE and light polarization. Although we have not considered excitonic effects, the energy regions from the paper of Gadret *et al.*³¹ can be mapped to our calculations with small QC and large WZ composition. When QC is increased, step like features are observed in the interband absorption for Z-polarization, which is parallel to the growth direction.

Since WZ and ZB present different optical selection rules, any mixing of these two crystal phases should combine these different light polarizations. Our DLP calculations for pure ZB or pure WZ are in good agreement with experiments of Mishra *et al.*,²⁹ and OC effects were necessary to match the experimental results. Stronger QC retains the WZ behavior of the DLP, since WZ HH has larger effective mass than ZB HH. In the polytypic cases, we found that the DLP is very susceptible to ZB regions and only a small amount of ZB drastically increases the DLP. This ZB susceptibility is increased if QC effects are decreased. Furthermore, our results for the DLP also explain the polarized PL measured by Gadret *et al.*³¹

In summary, we believe that our findings provide a theoretical explanation for the optical properties observed in InP polytypic superlattices and also indicate how linear light polarization can be tuned using QC and crystal phase mixing. We wish to emphasize that our theoretical approach is not only limited to InP but also could be applied to other III-V compounds that exhibit polytypism.⁴³

ACKNOWLEDGMENTS

The authors acknowledge financial support from the Brazilian agencies CNPq (Grant Nos. 138457/2011-5, 246549/2012-2, and 149904/2013-4) and FAPESP (Grant Nos. 2011/19333-4, 2012/05618-0, and 2013/23393-8). The authors thank James P. Parry and Karie Friedman for kindly proofreading the paper.

APPENDIX: SECOND-ORDER CORRECTIONS

When the interband coupling is considered in k·p Hamiltonians, it is necessary to correct some of the second order parameters due to the modification of states that belong to classes A and B.³⁵ For the Luttinger parameters in ZB, we have

$$\begin{aligned}\tilde{\gamma}_1 &= \gamma_1 - \frac{E_P}{3E_g} \\ \tilde{\gamma}_2 &= \gamma_2 - \frac{E_P}{6E_g} \\ \tilde{\gamma}_3 &= \gamma_3 - \frac{E_P}{6E_g} \\ F &= \frac{1}{m_e^*} - \frac{E_g + \frac{2}{3}\Delta_{SO}}{E_g + \Delta_{SO}} \frac{E_P}{E_g} \\ E_P &= \frac{2m_0}{\hbar^2} P^2\end{aligned}\quad (A1)$$

and for WZ parameters, we have

$$\begin{aligned}\tilde{A}_1 &= A_1 + \frac{E_{P1}}{E_g + \Delta_1} \\ \tilde{A}_2 &= A_2 \\ \tilde{A}_3 &= A_3 - \frac{E_{P1}}{E_g + \Delta_1} \\ \tilde{A}_4 &= A_4 + \frac{1}{2} \frac{E_{P2}}{E_g} \\ \tilde{A}_5 &= A_5 + \frac{1}{2} \frac{E_{P2}}{E_g} \\ \tilde{A}_6 &= A_6 + \frac{1}{\sqrt{2}} \frac{\sqrt{E_{P1}E_{P2}}}{E_g + \frac{\Delta_1}{2}} \\ \tilde{e}_1 &= e_1 - \frac{E_{P1}}{E_g + \Delta_1} \\ \tilde{e}_2 &= e_2 - \frac{E_{P2}}{E_g} \\ E_{P1(2)} &= \frac{2m_0}{\hbar^2} P_{1(2)}^2.\end{aligned}\quad (A2)$$

Given the corrected Luttinger parameters, we only have to connect them to the ones in the Hamiltonian (2), using the same idea as presented in our previous paper³³

$$\begin{aligned}\Delta_1 &= 0 \\ \Delta_2 &= \Delta_3 = \frac{\Delta_{SO}}{3} \\ \tilde{A}_1 &= -\tilde{\gamma}_1 - 4\tilde{\gamma}_3 \\ \tilde{A}_2 &= -\tilde{\gamma}_1 + 2\tilde{\gamma}_3 \\ \tilde{A}_3 &= 6\tilde{\gamma}_3 \\ \tilde{A}_4 &= -3\tilde{\gamma}_3 \\ \tilde{A}_5 &= -\tilde{\gamma}_2 - 2\tilde{\gamma}_3 \\ \tilde{A}_6 &= -\sqrt{2}(2\tilde{\gamma}_2 + \tilde{\gamma}_3) \\ \tilde{A}_z &= \tilde{\gamma}_2 - \tilde{\gamma}_3 \\ \tilde{e}_1 &= \tilde{e}_2 = F \\ P_1 &= P_2 = P\end{aligned}\quad (A3)$$

For the numerical values presented in Table I, we first corrected the ZB parameters and then applied the connection to the polytypic Hamiltonian.

¹P. Mohan, J. Motohisa, and T. Fukui, *Nanotechnology* **16**, 2903 (2005).

²T. T. Vu, T. Zehender, M. A. Verheijen, S. R. Plissard, G. W. G. Immink, J. E. M. Haverkort, and E. P. A. M. Bakkers, *Nanotechnology* **24**, 115705 (2013).

³D. Pan, M. Fu, X. Yu, X. Wang, L. Zhu, S. Nie, S. Wang, Q. Chen, P. Xiong, S. von Molnár, and J. Zhao, *Nano Lett.* **14**, 1214 (2014).

⁴S. Lehmann, J. Wallentin, D. Jacobsson, K. Deppert, and K. A. Dick, *Nano Lett.* **13**, 4099 (2013).

⁵V. Khranovskyy, A. M. Glushenkov, Y. Chen, A. Khalid, H. Zhang, L. Hultman, B. Monemar, and R. Yakimova, *Nanotechnology* **24**, 215202 (2013).

⁶F. Ren, K. Wei Ng, K. Li, H. Sun, and C. J. Chang-Hasnain, *Appl. Phys. Lett.* **102**, 012115 (2013).

⁷M. Borg, H. Schmid, K. E. Moselund, G. Signorello, L. Gignac, J. Bruley, C. Breslin, P. Das Kanungo, P. Werner, and H. Riel, *Nano Lett.* **14**, 1914 (2014).

⁸M. Heiss, E. Russo-Averchi, A. Dalmau-Mallorquí, G. Tütüncüoğlu, F. Matteini, D. Ruffer, S. Conesa-Boj, O. Demichel, E. Alarcon-Lladó, A. Fontcuberta, and I. Morral, *Nanotechnology* **25**, 014015 (2014).

- ⁹K. Li, H. Sun, F. Ren, K. W. Ng, T.-T. D. Tran, R. Chen, and C. J. Chang-Hasnain, *Nano Lett.* **14**, 183 (2014).
- ¹⁰N. Akopian, G. Patriarche, L. Liu, J.-C. Harmand, and V. Zwiller, *Nano Lett.* **10**, 1198 (2010).
- ¹¹M. Smit, X. Leijtens, H. Ambrosius, E. Bente, J. van der Tol, B. Smalbrugge, T. de Vries, E.-J. Geluk, J. Bolk, R. van Veldhoven, L. Augustin, P. Thijs, D. D'Agostino, H. Rabbani, K. Lawniczuk, S. Stopinski, S. Tahvili, A. Corradi, E. Kleijn, D. Dzibrou, M. Felicetti, E. Bitincka, V. Moskalenko, J. Zhao, R. Santos, G. Gilardi, W. Yao, K. Williams, P. Stabile, P. Kuindersma, J. Pello, S. Bhat, Y. Jiao, D. Heiss, G. Roelkens, M. Wale, P. Firth, F. Soares, N. Grote, M. Schell, H. Debregeas, M. Achouche, J.-L. Gentner, A. Bakker, T. Korthorst, D. Gallagher, A. Dabbs, A. Melloni, F. Morichetti, D. Melati, A. Wonfor, R. Penty, R. Broeke, B. Musk, and D. Robbins, *Semicond. Sci. Technol.* **29**, 083001 (2014).
- ¹²H. J. Joyce, C. J. Docherty, Q. Gao, H. H. Tan, C. Jagadish, J. Lloyd-Hughes, L. M. Herz, and M. B. Johnston, *Nanotechnology* **24**, 214006 (2013).
- ¹³C. S. Ponseca, H. Němec, J. Wallentin, N. Anttu, J. P. Beech, A. Iqbal, M. Borgström, M.-E. Pistol, L. Samuelson, and A. Yartsev, *Phys. Rev. B* **90**, 085405 (2014).
- ¹⁴M. Murayama and T. Nakayama, *Phys. Rev. B* **49**, 4710 (1994).
- ¹⁵T. Ba Hoang, A. F. Moses, L. Ahtapodov, H. Zhou, D. L. Dheeraj, A. T. J. van Helvoort, B.-O. Fimland, and H. Weman, *Nano Lett.* **10**, 2927 (2010).
- ¹⁶K. Pemasiri, M. Montazeri, R. Gass, L. M. Smith, H. E. Jackson, J. Yarrison-Rice, S. Paiman, Q. Gao, H. H. Tan, C. Jagadish, X. Zhang, and J. Zou, *Nano Lett.* **9**, 648 (2009).
- ¹⁷C. K. Yong, J. Wong-Leung, H. J. Joyce, J. Lloyd-Hughes, Q. Gao, H. H. Tan, C. Jagadish, M. B. Johnston, and L. M. Herz, *Nano Lett.* **13**, 4280 (2013).
- ¹⁸X. Duan, Y. Huang, Y. Cui, J. Wang, and C. M. Lieber, *Nature* **409**, 66 (2001).
- ¹⁹X. Jiang, Q. Xiong, S. Nam, F. Qian, Y. Li, and C. M. Lieber, *Nano Lett.* **7**, 3214 (2007).
- ²⁰J. Wallentin, M. Ek, L. R. Wallenberg, L. Samuelson, and M. T. Borgström, *Nano Lett.* **12**, 151 (2012).
- ²¹Z. Wang, B. Tian, M. Paladugu, M. Pantouvaki, N. Le Thomas, C. Merckling, W. Guo, J. Dekoster, J. Van Campenhout, P. Absil, and D. Van Thourhout, *Nano Lett.* **13**, 5063 (2013).
- ²²J. Wallentin, N. Anttu, D. Asoli, M. Huffman, I. Aberg, M. H. Magnusson, G. Siefer, P. Fuss-Kailuweit, F. Dimroth, B. Witzigmann, H. Q. Xu, L. Samuelson, K. Deppert, and M. T. Borgström, *Science* **339**, 1057 (2013).
- ²³Y. Cui, J. Wang, S. R. Plissard, A. Cavalli, T. T. T. Vu, R. P. J. van Veldhoven, L. Gao, M. Trainor, M. A. Verheijen, J. E. M. Haverkort, and E. P. A. M. Bakkers, *Nano Lett.* **13**, 4113 (2013).
- ²⁴T. Akiyama, K. Nakamura, and T. Ito, *Phys. Rev. B* **73**, 235308 (2006).
- ²⁵Y. Kitauchi, Y. Kobayashi, K. Tomioka, S. Hara, K. Hiruma, T. Fukui, and J. Motohisa, *Nano Lett.* **10**, 1699 (2010).
- ²⁶K. Ikejiri, Y. Kitauchi, K. Tomioka, J. Motohisa, and T. Fukui, *Nano Lett.* **11**, 4314 (2011).
- ²⁷P. J. Poole, D. Dalacu, X. Wu, J. Lapointe, and K. Mnaymneh, *Nanotechnology* **23**, 385205 (2012).
- ²⁸M. Mattila, T. Hakkarainen, M. Mulot, and H. Lipsanen, *Nanotechnology* **17**, 1580 (2006).
- ²⁹A. Mishra, L. V. Titova, T. B. Hoang, H. E. Jackson, L. M. Smith, J. M. Yarrison-Rice, Y. Kim, H. J. Joyce, Q. Gao, H. H. Tan, and C. Jagadish, *Appl. Phys. Lett.* **91**, 263104 (2007).
- ³⁰S. Paiman, Q. Gao, H. H. Tan, C. Jagadish, K. Pemasiri, M. Montazeri, H. E. Jackson, L. M. Smith, J. M. Yarrison-Rice, X. Zhang, and J. Zou, *Nanotechnology* **20**, 225606 (2009).
- ³¹E. G. Gadret, G. O. Dias, L. C. O. Dacal, M. M. de Lima, C. V. R. S. Ruffo, F. Iikawa, M. J. S. P. Brasil, T. Chiamonte, M. A. Cotta, L. H. G. Tizei, D. Ugarte, and A. Cantarero, *Phys. Rev. B* **82**, 125327 (2010).
- ³²P. Kailuweit, M. Peters, J. Leene, K. Mergenthaler, F. Dimroth, and A. W. Bett, *Prog. Photovoltaics: Res. Appl.* **20**, 945 (2012).
- ³³P. E. Faria Junior and G. M. Sipahi, *J. Appl. Phys.* **112**, 103716 (2012).
- ³⁴S. H. Park and S. L. Chuang, *J. Appl. Phys.* **87**, 353 (2000).
- ³⁵P. Löwdin, *J. Chem. Phys.* **19**, 1396 (1951).
- ³⁶G. Bastard, *Phys. Rev. B* **24**, 5693 (1981).
- ³⁷G. Baraff and D. Gershoni, *Phys. Rev. B* **43**, 4011 (1991).
- ³⁸S. L. Chuang, *Physics of Optoelectronic Devices* (John Wiley, New York, 1995).
- ³⁹V. V. Ravi Kishore, B. Partoens, and F. M. Peeters, *Phys. Rev. B* **82**, 235425 (2010).
- ⁴⁰M. Califano and A. Zunger, *Phys. Rev. B* **70**, 165317 (2004).
- ⁴¹J. Wang, M. S. Gudiksen, X. Duan, Y. Cui, and C. M. Lieber, *Science* **293**, 1455 (2001).
- ⁴²M. P. Persson and H. Q. Xu, *Phys. Rev. B* **70**, 161310 (2004).
- ⁴³A. De and C. E. Pryor, *Phys. Rev. B* **81**, 155210 (2010).
- ⁴⁴S. L. Chuang and C. S. Chang, *Appl. Phys. Lett.* **68**, 1657 (1996).